PHYSICAL REVIEW B **87**, 085403 (2013)

Self-organized chromium oxide monolayers on Fe(001)

A. Picone,[1] G. Fratesi,[2] M. Riva,[1] G. Bussetti,[1] A. Calloni,[1] A. Brambilla,[1] M. I. Trioni,[3] L. Duò,[1] F. Ciccacci,[1] and M. Finazzi[1]

[1]*CNISM, Dipartimento di Fisica, Politecnico di Milano, Piazza Leonardo da Vinci 32, 20133 Milano, Italy*

[2]*Dipartimento di Scienza dei Materiali, Università di Milano-Bicocca, Via Cozzi 53, 20125 Milano, Italy*

[3]*CNR - National Research Council of Italy, ISTM, via Golgi 19, 20133, Milano, Italy*

(Received 13 December 2012; published 4 February 2013)

The oxygen-saturated Fe(001)-$p(1 \times 1)$O surface has been used as a template to stabilize two-dimensional Cr oxides on Fe(001). Cr deposition at 400 °C leads to two different well-ordered phases, depending on the amount of Cr deposited. In the submonolayer regime a novel $c(4 \times 2)$ overlayer self-assembles on the Fe(001)-$p(1 \times 1)$O surface, saturating for a coverage of about 0.75 monolayers. This phase becomes unstable for higher coverages, when a $(\sqrt{5} \times \sqrt{5})R27^\circ$ superstructure emerges. The structural and electronic details of the two one-layer-thick oxides are studied by combining high-resolution scanning tunneling microscopy, low-energy electron diffraction, Auger electron spectroscopy, and density functional theory.

DOI: 10.1103/PhysRevB.87.085403 PACS number(s): 68.37.Ef, 75.47.Lx, 68.55.J−, 68.47.Gh

I. INTRODUCTION

The growth of thin epitaxial oxide films on metal supports is attracting considerable scientific interest both on a fundamental level and for potential technological applications.[1–9] In particular, the structural characterization of oxide structures is of crucial importance in order to get insight into the chemical and physical processes occuring in a variety of modern technological devices based on ultrathin oxide films, such as solid-state electronic devices, high-storage-density media, and metal oxide catalysts. In this respect scanning tunneling microscopy (STM) and theoretical modeling through density functional theory (DFT) calculations have proven to be a powerful combination to disentangle the atomic structure of well-defined oxide surfaces supported by metals.[10]

Among ultrathin oxide films, particular effort has been devoted to the investigation of single-layer oxides.[11] The interest in one-layer-thick oxides is manifold, in particular (i) two-dimensional oxides can be seen as model systems for the oxide/metal interface, allowing investigation by means of high-resolution scanning probe techniques; (ii) the vertical confinement and the elastic and electronic coupling with the metallic substrate allows stabilizing stoichiometries and atomic structures that can differ with respect to the corresponding bulk terminations, with important implications in chemical reactivity,[12,13] adsorption properties,[14] and magnetic ordering[15] of the resulting structures; and (iii) the wetting layer can represent the precursor phase for the growth of thicker films.[16,17]

Single layers of transition metal oxides have been stabilized on noble and quasinoble metals such as, for instance, Pd,[18,19] Ag,[20,21] Pt,[22,23] Au,[24] and Ir.[25] In these cases, growth techniques such as reactive deposition (i.e., metal deposition in oxygen atmosphere) and/or postoxidation are typically applied, leading to ordered phases and well-defined oxide-metal interfaces. On the contrary, when a more reactive metal, such as Fe, is used as a substrate for the nano-oxide growth, these procedures fail to produce sharp metal/oxide interfaces. Indeed, during the metal deposition in oxygen atmosphere, extensive and uncontrolled oxidation of Fe occurs, preventing the stabilization of long-range ordered oxide monolayers.[26,27] However, the study of Fe-supported two dimensional oxides is a relevant topic since, besides the elastic and the electronic coupling with the substrate, the magnetic coupling also can influence the stabilization and the physical properties of the nano-oxide phases.[1]

An alternative route to obtain a sharp interface between a single layer of transition metal oxide and a reactive substrate may be to exploit the oxygen adsorbed on the surface before metal deposition since, in this case, the amount of oxygen available is well defined. Preloaded oxygen on surface and subsurface sites has been used for the preparation of two-dimensional films of vanadium, niobium, and molybdenum oxides on $Cu_3Au(100)$[28] and, more recently, to obtain a sharp interface between a Ni thin film and a single layer of NiO.[29]

The well-ordered and defect-free Fe(001)-$p(1 \times 1)$O surface is an ideal template to implement this strategy.[30–36] The surface is characterized by one oxygen atom per surface unit cell, which can be used as a reservoir for the stabilization of two-dimensional transition metal oxides. Furthermore, the atomic structure of the Fe(001)-$p(1 \times 1)$O surface has been suggested to be similar to an ultrathin rocksalt-type FeO film.[31,37]

Among the transition metal ultrathin oxide films, Cr oxide is one of the less investigated (see, for instance, Refs. 38–42). Chromium oxide forms stable phases in the bulk with different structures, stoichiometry, and properties. For example, Cr_2O_3 is an antiferromagnetic insulator while CrO_2 is a half-metallic ferromagnetic material. In addition, when chromium oxide is prepared in the form of an ultrathin film, structures not directly associated with stable bulk phases have also been obtained. For instance, although the rocksalt-type CrO does not exist in the bulk, the surface structure resulting from the first layer of Cr oxide grown on Cu(110) is ascribed to a CrO(111)-like oxide, with the cations in the formal Cr^{2+} oxidation state.[43] Another example is given by Cr deposition onto a water precovered Cu(111) surface, a procedure that leads to the stabilization of a new type of chromium oxide with a square two-dimensional lattice.[44]

In this paper we show how the Fe(001)-$p(1 \times 1)$O surface can be used as a template for the self assembly of two dimensional Cr_xO_y oxides. Cr deposition on this surface

leads to two different phases, depending on the amount of deposited Cr. At 0.75 monolayers coverage a $c(4 \times 2)$ overlayer with Cr_3O_4 formal stoichiometry is stabilized, while a $(\sqrt{5} \times \sqrt{5})R27^\circ$ superstructure with Cr_4O_5 stoichiometry is obtained at slightly higher coverages.

II. EXPERIMENT

Samples were prepared in an ultrahigh vacuum (UHV) system (low 10^{-10} mbar pressure range) by starting from a UHV-cleaned MgO(001) single crystal substrate, over which a 200-nm-thick Fe(001) film was grown by means of molecular beam epitaxy (MBE).

Fe(001)-$p(1 \times 1)$O surfaces were obtained by exposing a clean Fe(001) substrate held at 500 °C to 30 langmuir (40×10^{-6} mbar×s) of pure O_2 (partial pressure: 2.0×10^{-7} mbar). The samples were then heated at 600 °C for 10 min to remove the excess oxygen from the surface. Oxygen chemisorption on the Fe(001) surface followed by annealing resulted in the oxygen-saturated and well-ordered Fe(001)-$p(1 \times 1)$O superstructure, characterized by one oxygen atom per surface unit cell, lying in the fourfold hollow site of the Fe surface.[33,45] Cr films were grown onto Fe(001)-$p(1 \times 1)$O substrates by MBE under UHV conditions, with a typical growth rate of about 1 equivalent monolayer[46] (ML) per minute, as measured by a quartz microbalance. In the set of measurements discussed in this paper the substrate was held at 400 °C during Cr deposition, as measured by a thermocouple attached in close proximity to the sample position. We also performed Cr deposition at lower substrate temperatures, down to 100 °C.[47] We observed that up to 300 °C island nucleation takes place, while deposition at 400 °C leads to an atomically flat and highly ordered surface.

The STM measurements were performed by using an Omicron variable temperature STM in a UHV chamber connected to the preparation system. STM images were acquired at room temperature in constant-current mode with home-made electrochemically etched W tips.

The low-energy electron diffraction (LEED) and Auger electron spectroscopy (AES) analysis was performed by means of a Omicron SPECTALEED with a retarding field analyzer (total acceptance angle 102°). A 3-kV, 20-μA electron beam was used, with a 3-V peak-to-peak modulation amplitude.

III. THEORY

The theoretical analysis is based on first-principle density functional theory (DFT) simulations with the generalized gradient approximation for the exchange and correlation functional as proposed by Perdew, Burke, and Ernzerhof (GGA-PBE),[48] taking into account the spin polarization in a collinear description. We adopted a repeated slab model with four Fe(001) layers, the bottom two fixed at the bulk spacing. Adsorbates were placed on the other side of the slab and fully relaxed together with two topmost Fe layers. A vacuum region of 12 Å separates repeated slabs from each other. The plane-wave ultrasoft pseudopotential method[49] was used as implemented in the PWSCF code of the Quantum-ESPRESSO distribution.[50] Pseudopotentials were generated starting from scalar-relativistic all-electron atomic calculations and using nonlinear core corrections. Semicore $3s3p$ states are included for Cr. Kinetic energy cutoffs are 55 Ry for the wave functions and 280 Ry for the effective potential and the charge density. The surface Brillouin zone sampling has been performed with the Monkhorst-Pack[51] scheme, adopting integration meshes equivalent to at least a 14×14 mesh in the irreducible surface unit cell of Fe(001). STM images have eventually been simulated within the Tersoff-Hamann approximation[52] by evaluating the Kohn-Sham local density of states in the energy interval between -1 eV and the Fermi level (analogous results were found at $+1$ eV), at constant height.

The stability of different structures is compared by evaluating the formation energy (per Cr atom) defined as

$$F = \frac{E^{\mathrm{tot}} - E^{\mathrm{tot}}_{\mathrm{Fe}\text{-}p(1\times1)\mathrm{O}} - \mu_{\mathrm{Cr}} N_{\mathrm{Cr}} - \mu_{\mathrm{Fe}} N_{\mathrm{Fe}}}{N_{\mathrm{Cr}}}, \qquad (1)$$

where E^{tot} is the total energy of the structure under consideration, $E^{\mathrm{tot}}_{\mathrm{Fe}\text{-}p(1\times1)\mathrm{O}}$ that of the Fe(001)-$p(1 \times 1)$O substrate, μ_{Cr} (μ_{Fe}) the total energy per atom of bulk Cr (Fe). Finally, N_{Cr} and N_{Fe} are the number of Cr and Fe atoms added on the substrate. The formation energy per surface area is given as F times the Cr coverage.

IV. RESULTS

Figure 1 focuses on a set of depositions performed with the substrate kept at 400 °C, for Cr coverages ranging from 0.1 to 0.8 ML.

At very low coverages, below 0.1 ML [see Fig. 1(a)] isolated atomic-scale protrusions are randomly distributed on the substrate. These small features are only seen after depositing Cr and thus can be related to the presence of Cr atoms, while the Cr-free surface appears extremely flat and defect free.[34] In constant current topographic images they appear as broad features (with atomic-scale widths of about 0.5 nm) and it was not possible to establish their position with respect to the underlying substrate lattice. Different tunneling conditions have been used for imaging, giving a positive corrugation ranging from 0.3 to 1 Å. We never imaged Cr atoms as topographic depressions. At this coverage the LEED diffraction pattern [Fig. 1(b)] exhibits a $p(1 \times 1)$ periodicity. The observation of these features in STM measurement performed at room temperature, where adatoms are usually extremely mobile, suggests that deposited Cr atoms could be blocked by embedding into the topmost substrate layers, similarly to what has been proposed for Cr grown on Fe(001).[53] We recall that the Fe(001)-$p(1 \times 1)$O substrate does not posses any preferential site for the atom stabilization (exploited, for example, in Ref. 54). We should mention that the oxygen adlayer could hinder the Cr atoms mobility; however, our previous measurements[47] demonstrate that the oxygen does not affect the Cr intralayer mass transport.

For a coverage of 0.4 ML, a careful inspection of the STM image reported in Fig. 1(c) shows that in the regions of the surface where the Cr density is higher some patches of a $c(4 \times 2)$ reconstruction are visible. This is supported by the LEED pattern, characterized by a faint $c(4 \times 2)$ superstructure [see Fig. 1(d)], indicating that the overlayer is locally ordered.

Well-ordered structures can be obtained at larger coverages. At 0.75 ML the substrate is entirely covered by an atomically

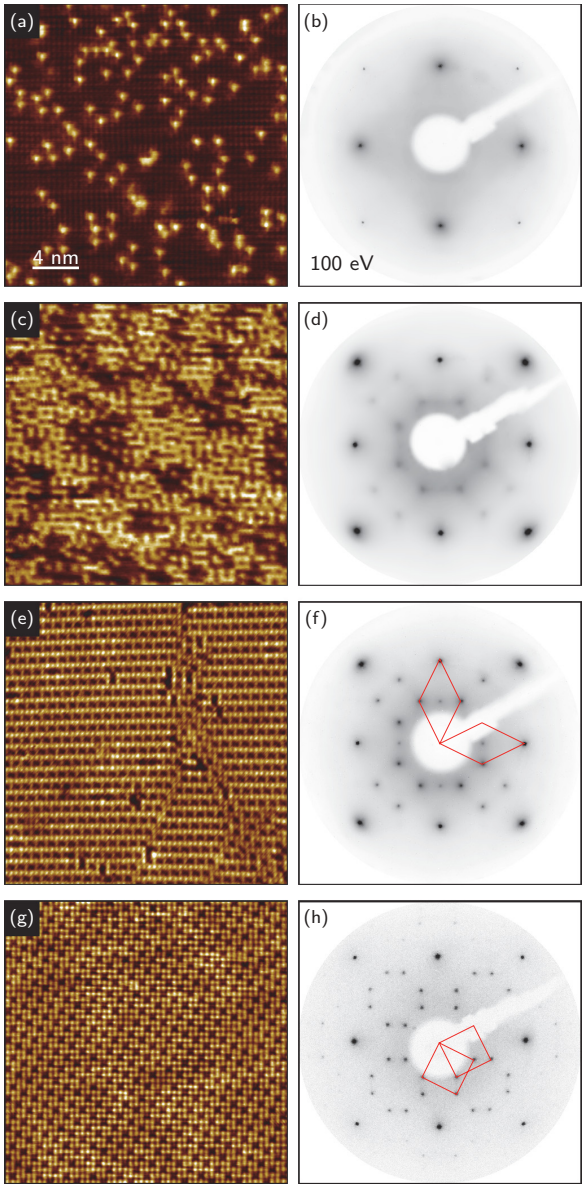

FIG. 1. (Color online) Left column: atomically resolved STM images after deposition of (a) 0.1, (c) 0.4, (e) 0.75, and (g) 0.8 ML of Cr on Fe(001)-$p(1 \times 1)$O, respectively ($I = 5$ nA, $V = 100$ mV). In the right column the corresponding LEED patterns (electron beam energy $E = 100$ eV) are reported. The reciprocal unit cells of the two rotational domains are superimposed on panels (f) and (h).

flat overlayer with a $c(4 \times 2)$ periodicity [see Fig. 1(e)] arising from an ordered array of dark holes with a rhombic primitive cell. The corresponding LEED pattern in Fig. 1(f) clearly shows extremely sharp spots with $c(4 \times 2)$ superstructure. Exceding the 0.75-ML coverage (by adding a mere 0.05 ML) leads to a large-scale reorganization of the overlayer, resulting in a transition toward a $(\sqrt{5} \times \sqrt{5})R27^\circ$ phase [see Figs. 1(g) and 1(h)]. The $c(4 \times 2)$ and the $(\sqrt{5} \times \sqrt{5})R27^\circ$ phases are characterized by a remarkable long range order, as visible in the STM images, showing large regions covered by a single domain. Furthermore, the LEED results show the presence of two equivalent domains for both phases, originating from the fourfold symmetry of the substrate.

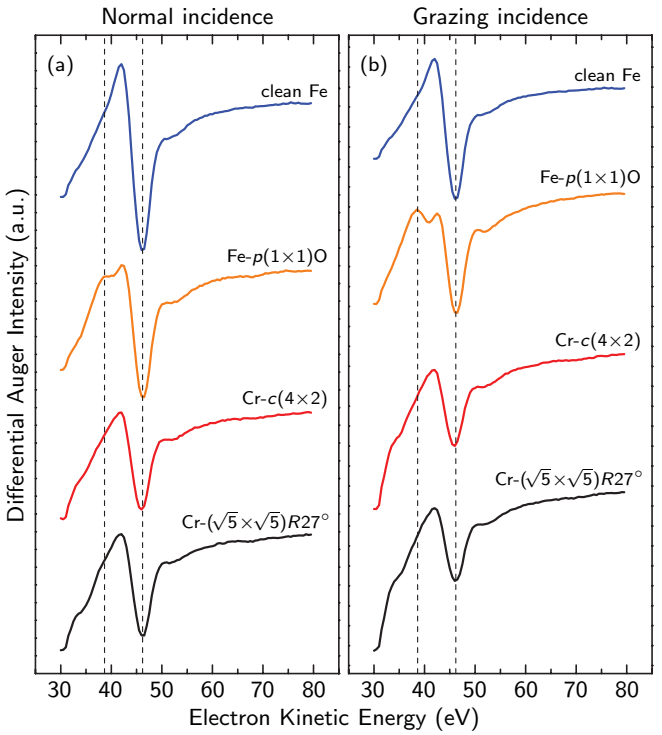

FIG. 2. (Color online) (a) Variation of the Fe(MNN) AES line shape at normal incidence for the different phases observed. (b) Same spectra with the sample normal tilted with respect to the incident beam current by an angle of 77°.

Eventually, at coverages well above 1 ML the $(\sqrt{5} \times \sqrt{5})R27^\circ$ periodicity persists, but the growth is characterized by the development of spirals.[47] Due to the increased surface roughness, the LEED pattern becomes weaker and high-quality STM images could not be obtained.

While the $(\sqrt{5} \times \sqrt{5})R27^\circ$ superstructure has already been observed for Cr(001) covered by one monolayer of oxygen,[55] a $c(4 \times 2)$ reconstruction is a new phase for Cr oxide stabilized by the interface with Fe(001). From STM measurements it is not possible to directly establish if the depressions are vacancies or atoms of another species (here, Fe), giving different STM contrast. We performed STM measurements using different tunneling conditions on both structures and we never imaged the $c(4 \times 2)$ or $(\sqrt{5} \times \sqrt{5})R27^\circ$ network as protrusions.

In order to get information about the chemistry of the interface we performed AES measurements. In Fig. 2 we show the low-energy Auger spectra taken on oxygen-free Fe(001), on Fe(001)-$p(1 \times 1)$O, and on the $c(4 \times 2)$ and $(\sqrt{5} \times \sqrt{5})R27^\circ$ phases. These low-energy peaks, corresponding to Fe(MNN) Auger transitions, are especially useful since their line shape has proven to be extremely sensitive to the chemical environment, in particular to Fe oxidation.[56] Comparison of the Auger spectra acquired on oxygen-free and oxidized Fe reveals that on the oxidized sample a shoulder appears at lower kinetic energy with respect to the main peak located at 47 eV, the latter being characteristic of oxygen-free Fe. This feature is more evident for Auger spectra performed at grazing incidence and can be considered as a fingerprint of the presence of O-Fe bonds in the topmost layer of the Fe(001)-$p(1 \times 1)$O surface. After Cr deposition the Auger peak

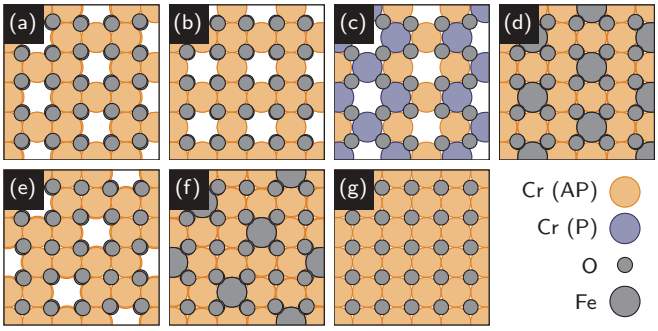

FIG. 3. (Color online) Top view of structures simulated by DFT: (a) $c(4 \times 2)$ phase with metal vacancies, (b) $p(2 \times 2)$, (c) $p(4 \times 2)$, (d) $c(4 \times 2)$ with Fe atoms filling the vacancies, (e) $(\sqrt{5} \times \sqrt{5})R27^\circ$ with metal vacancies, (f) $(\sqrt{5} \times \sqrt{5})R27^\circ$ with Fe atoms filling the vacancies, and (g) $p(1 \times 1)$. Only atoms above the Fe(001) surface layer are depicted. Cr (AP)/(P) refer to atoms with magnetic moment antiparallel/parallel to the one of the Fe surface.

recovers the characteristic line shape of oxygen-free Fe. This implies that iron is no more bound to oxygen atoms, even though the amount of oxygen has not changed, as checked by measuring the intensity of the O(KLL) transition (not shown). We thus have a definite experimental evidence that oxygen is bound only to Cr atoms and that the two observed phases are wetting layers of Cr oxide accomodated on top of the Fe(001) surface.

To better understand the atomistic and electronic properties of the observed Cr oxide superstructures, we have analyzed a few structural models by use of DFT calculations, depicted in Figs. 3(a)–3(g). Cr atoms were placed in the hollow sites of the Fe(001) surface, originally occupied by oxygen

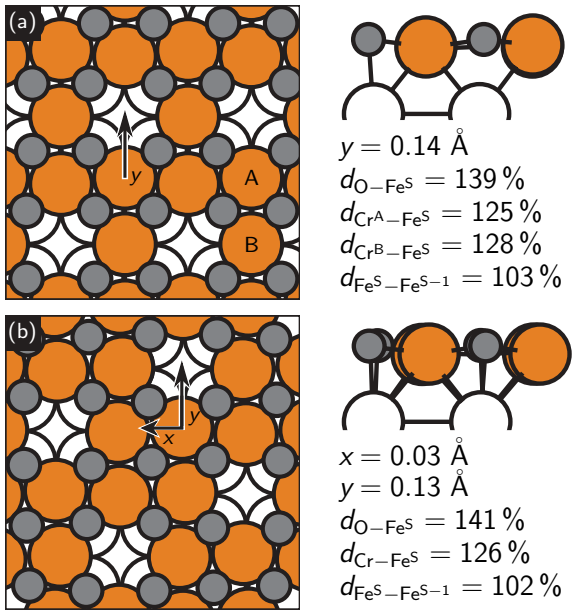

FIG. 4. (Color online) Top and side views of the (a) $c(4 \times 2)$ and (b) $(\sqrt{5} \times \sqrt{5})R27^\circ$ phases. The arrows indicate the in-plane displacements (x, y) of Cr atoms. Interlayer spacings d are given in percentages of that in bulk iron. By Fe^S and Fe^{S-1} we indicate iron atoms in the first and second layer, respectively.

TABLE I. Summary of DFT energetics. The unit cell of each structure covers $N_{1\times1}$ primitive unit cells of Fe(001) and includes N_{Cr} (N_{Fe}) Cr (Fe) atoms. F indicates the formation energy per Cr atom; see Eq. (1). Refer to Fig. 3 for structural models.

Coverage	Structure	Periodicity	$N_{1\times1}$	N_{Cr}	N_{Fe}	F (eV)
0.75 ML	(a)	$c(4 \times 2)$	4	3	0	−1.12
	(b)	$p(2 \times 2)$	4	3	0	−1.05
	(c)[a]	$p(4 \times 2)$	8	6	0	−0.99
	(d)[b]	$c(4 \times 2)$	4	3	1	−0.70
0.80 ML	(e)	$(\sqrt{5} \times \sqrt{5})R27^\circ$	5	4	0	−1.02
	(f)[b]	$(\sqrt{5} \times \sqrt{5})R27^\circ$	5	4	1	−0.69
1.00 ML	(g)	$p(1 \times 1)$	1	1	0	−0.55

[a]Antiferromagnetic coupling within the Cr layer.
[b]Vacancies filled by Fe atoms.

atoms. The latter occupy Fe-atop sites, between Cr atoms and slightly above them (see below). This O-Cr-Fe(001) arrangement is consistent with the AES findings showing no Fe-O bonds and with our calculations for trial 1-ML structures. In fact, a simulation with the order of layers initially set to Cr-O-Fe(001) eventually resulted in O-Cr-Fe(001) without any energy barrier. Moreover, displacing the oxide layer in the plane, to have Cr atop Fe atoms, has an energy cost of 0.39 eV per Cr atom. Unless specified, the magnetic moment of all Cr atoms will be parallel to each other and antiparallel to the one of the Fe surface (antiferromagnetic Cr-Fe coupling).

The formation energy per Cr atom calculated for each structure is reported in Table I. For a 0.75-ML Cr coverage, the most stable arrangement is the $c(4 \times 2)$ structure where the topmost layer is composed 75% by Cr atoms and 25% by vacancies, see Fig. 3(a), as suggested by the experimental findings. Such a result agrees with the observation of the $c(4 \times 2)$ periodicity in the early nucleation stages, see Fig. 1(c), while for example a (1×1) local order, structure (g), requires further 0.57 eV per Cr atom. Comparing other structures with a 0.75-ML Cr coverage, a $p(2 \times 2)$ overlayer, sketched in Fig. 3(b), is less stable by 0.07 eV per Cr atom. As the antiferromagnetic Cr-Fe coupling induces magnetic frustration among the Cr atoms, preventing them to have spin antiparallel to those of their nearest neighbors, we have considered a $p(4 \times 2)$ structure such as that in Fig. 3(c). There, Cr atoms take about the same positions as in the $c(4 \times 2)$, but with Cr magnetic moments alternately parallel/antiparallel to that of Fe. This magnetic configuration is less convenient (by 0.13 eV/Cr atom) with respect to the one with Cr spins all antiparallel to the Fe magnetization, showing that the coupling with the substrate is dominant. Finally, to disclose the nature of the depressions observed in the STM, we consider a 0.75-ML model where Fe atoms are trapped from the substrate into the 25% vacancy sites. This structure, shown in Fig. 3(d), has the right $c(4 \times 2)$ periodicity and could be compatible with the STM observations; however, its formation energy makes it highly unfavorable, with an energy cost per Fe atom estimated as $N_{Cr}[F^{(d)} - F^{(a)}] = 1.27$ eV.

The morphology and main structural parameters of the most stable $c(4 \times 2)$ overlayer [Fig. 3(a)] are summarized in Fig. 4(a). Two inequivalent Cr atoms are present on the surface, denoted by Cr^A and Cr^B, which have three and two nearest

Cr neighbors, respectively. They differ by the net charge (as determined by Löwdin population analysis[57]) and the magnetic moment, which are $+1.12\ e$ ($+1.16\ e$) and $2.9\ \mu_B$ ($3.1\ \mu_B$), respectively, for Cr^A (Cr^B). Notice that the magnetic moment is higher for Cr^B, which, having a lower number of Cr neighbors, is less affected by magnetic frustration. Electrons displaced from positively charged Cr atoms mostly move toward the oxygen atoms, which become negatively charged ($-0.62\ e$ each). Some charge also flows toward the first Fe layer ($-0.08\ e$ per Fe atom). Hence, a positively charged oxide layer is supported by a negatively charged substrate. As pointed out in Ref. 58, these are the conditions to observe rumpling of the supported oxide film, with the anion sublayer at larger distances from the support than the cation one, as we found also in our case. Indeed, the layer of O atoms protrudes over the Cr one by $d_{O-Cr} = 26\%$ [here and in the following interlayer distances are given in terms of percentages of the one of bulk Fe(001), i.e., $d = 100\%$ corresponds to 1.43 Å]. One further notices a considerable expansion of the Cr-Fe distance, (d_{Cr-Fe}), similarly to the case of 1 ML of oxygen deposited on either pure Fe(001)[30] or Cr(001).[59] More specifically, we found $d_{Cr-Fe} = 125\%$. Finally, Cr^A atoms are displaced from the hollow site by 0.14 Å and are 0.04 Å lower on the surface than Cr^B. The O-Cr distance is 1.97 Å (1.99 Å) for A (B) atoms, larger than that in chromium oxides (e.g., 1.88 Å in CrO_2[60]). Simulated STM images, reported in Fig. 5(a), show bright spots located above the chromium atoms and dark areas above Cr vacancies, in excellent agreement with experiments [Fig. 5(c)]. A small contrast between Cr^A and Cr^B can be detected both in the simulations and the experimental data.

We now move to the case corresponding to a coverage of 0.80 ML and consider a $(\sqrt{5} \times \sqrt{5})R27^\circ$ superstructure, depicted in Fig. 3(e). For this coverage we obtain $F^{(e)} = -1.02$ eV. This value can be compared to the formation energy we obtain by filling 20% of the $c(4 \times 2)$ vacancy sites with Cr atoms to obtain 0.80-ML coverage. In this case 25% of the Cr atoms form $p(1 \times 1)$ patches within the $c(4 \times 2)$ phase, yielding $F^{mix} = 0.75F^{(a)} + 0.25F^{(g)} = -0.98$ eV. The difference in the formation energies [$F^{mix} > F^{(e)}$] agrees with the experimental observation of the abrupt phase transition from $c(4 \times 2)$ to $(\sqrt{5} \times \sqrt{5})R27^\circ$. A detailed view with geometric parameters is provided in Fig. 4(b). All Cr atoms are now equivalent, with a Löwdin charge equal to $+1.12\ e$ and a magnetic moment of $3.0\ \mu_B$. They are displaced from the hollow sites by 0.13 and 0.03 Å in the two directions [see Fig. 4(b)]. This is very similar to what has been reported for the $(\sqrt{5} \times \sqrt{5})R27^\circ$ on O-dosed Cr(001).[59] The O-Cr distance is 2.09/1.95 Å, the larger value for oxygen atoms at the center of Cr squares. The simulated STM image [Fig. 5(b)] is again in excellent agreement with experimental findings [Fig. 5(d)]. Finally, it is interesting to notice that, similarly to the $c(4 \times 2)$ case, the occupation of vacancy sites by Fe atoms, as schematically depicted in Fig. 3(f), would increase significantly the formation energy, here by $N_{Cr}[F^{(f)} - F^{(e)}] = 1.34$ eV per added Fe atom.

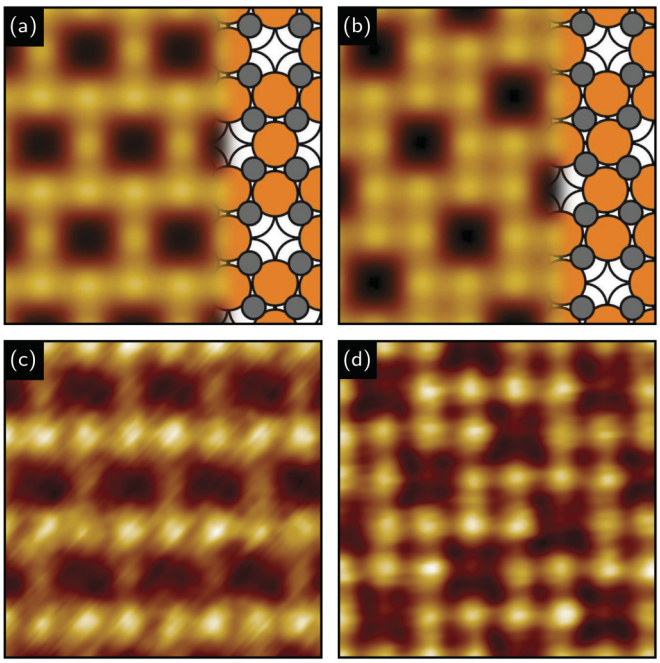

FIG. 5. (Color online) Simulated [(a) and (b)] and experimental [(c) and (d)] STM of the $c(4 \times 2)$ and $(\sqrt{5} \times \sqrt{5})R27^\circ$ phases.

V. DISCUSSION

The mechanism behind the formation of the ordered networks of cation vacancies deserves some attention and is qualitatively discussed here in comparison with the literature. We recall that a $c(4 \times 2)$ superstructure like the one observed here has been reported for a number of rocksalt-type oxides on Pd(001).[19,61,62] In those cases, the occurrence of metal vacancies has been proposed as a mechanism able to compensate the compressive stress due to a large lattice mismatch between the substrate and the overlayer. In the present case, however, the interfacial strain is unlikely to be relevant in inducing cation vacancies. Indeed, as pointed out by Schmid *et al.*, a hypothetical rocksalt-like CrO should have a lattice constant of approximately 4.08 Å,[55] in good agreement with the Fe(001) lattice in the [110] direction (4.05 Å).

Another possibility would be intervention of electronic effect, as advocated by Eichler and Hafner[59] to explain the mechanism for surface vacancy formation in Cr(001) following 1-ML adsorption of oxygen. It was found that the presence of the adsorbates increases the filling of the spin-majority $d_{x^2-y^2}$ states, which are directed along the Cr-Cr bond direction: as a consequence, electron states with antibonding character in between Cr atoms are also filled, destabilizing the overlayer; conversely, the spin-minority states $d_{x^2-y^2}$, including those with bonding character, are emptied. In close analogy with their analysis, we found that for the one-layer-thick CrO on Fe(001) (in both phases) the spin-majority and spin-minority $d_{x^2-y^2}$ are completely filled and empty, respectively, so the same mechanism is expected to be relevant in our case.

A further effect can be related to magnetic interactions. The antiferromagnetic ordering of bulk Cr is characterized by in-plane ferromagnetic (001) layers, but a free-standing Cr(001) plane would prefer to be antiferromagnetic. As we have seen for the case of the $c(4 \times 2)$ phase, coupling to the substrate is stronger and induces the Cr spins to be antiparallel to those of Fe, therefore implying magnetic frustration between

nearby Cr atoms. Vacancies contribute to releasing some of this frustration by reducing the number of nearest neighbors. The picture that has been outlined above could be further corroborated by direct investigation of the magnetic properties of the Cr oxide layer, e.g., by means of x-ray magnetic dichroism.

Finally, it is interesting to notice that no $c(4 \times 2)$ surface structure was observed for the 1-ML-thick CrO supported by Cr(001), which only shows the $(\sqrt{5} \times \sqrt{5})R27^\circ$ periodicity.[55] We have no quantitative arguments to motivate the difference between Fe and Cr substrates, but we point out that the surface lattice constant of Fe(001) is 0.04 Å smaller than that of Cr(001). With shorter Cr-Cr distances on the iron support, both the electronic and the magnetic argument for the formation of vacancies should become more important, thus with a stronger effect on the $c(4 \times 2)$ phase than on the $(\sqrt{5} \times \sqrt{5})R27^\circ$ one.

VI. CONCLUSIONS

In conclusion, high-temperature deposition of Cr onto the oxygen saturated Fe(001)-$p(1 \times 1)$O leads to the self-assembling of two highly ordered one-layer-thick Cr oxides, characterized by $c(4 \times 2)$ and $(\sqrt{5} \times \sqrt{5})R27^\circ$ periodicity, respectively, depending on Cr coverage. Long-range order is demonstrated by high-resolution STM images and LEED, while AES shows that Cr-O bonds have replaced Fe-O ones. Theoretical calculations reveal that both phases arise from an ordered array of Cr vacancies in the oxide layer, leading to Cr_3O_4 and Cr_4O_5 formal stoichiometries. The oxide layers are positively charged and rumpled with anions protruding above cations. The highly ordered array of vacancies in the oxide layer could be further exploited to realize the template-assisted self-assembly of metal nanoparticles,[63] here on a magnetic substrate.

ACKNOWLEDGMENTS

This work was partially supported by the Italian Ministry of University and Research trough the FIRB project RBAP115AYN. Computational resources were made available in part by CINECA (application code HP10C3YWUA).

[1] M. Finazzi, L. Duò, and F. Ciccacci, Surf. Sci. Rep. **64**, 139 (2009).
[2] F. P. Netzer, F. Allegretti, and S. Surnev, J. Vac. Sci. Technol. B **28**, 1 (2010).
[3] M. Finazzi, L. Duò, and F. Ciccacci, eds., *Magnetic Properties of Antiferromagnetic Oxide Materials: Surfaces, Interfaces and Thin Films* (Wiley-VCH Verlag, Weinheim, 2010).
[4] S. Valeri and G. Pacchioni, eds., *Oxide Ultrathin Films* (Wiley-VCH Verlag, Weinheim, 2011).
[5] U. Diebold, S.-C. Li, and M. Schmid, Annu. Rev. Phys. Chem. **61**, 129 (2010).
[6] G. Pacchioni, Chem. Eur. J. **18**, 10144 (2012).
[7] N. Nilius, Surf. Sci. Rep. **64**, 595 (2009).
[8] S. A. Chambers, Surf. Sci. Rep. **39**, 105 (2000).
[9] C. T. Campbell, Surf. Sci. Rep. **27**, 1 (1997).
[10] M. Sierka, Prog. Surf. Sci. **85**, 398 (2010).
[11] F. P. Netzer, Surf. Sci. **604**, 485 (2010).
[12] Y.-N. Sun, Z.-H. Qin, M. Lewandowski, E. Carrasco, M. Sterrer, S. Shaikhutdinov, and H.-J. Freund, J. Catal. **266**, 359 (2009).
[13] S. Altieri, S. F. Contri, and S. Valeri, Phys. Rev. B **76**, 205413 (2007).
[14] N. Nilius, E. D. L. Rienks, H.-P. Rust, and H.-J. Freund, Phys. Rev. Lett. **95**, 066101 (2005).
[15] F. Mittendorfer, M. Weinert, R. Podloucky, and J. Redinger, Phys. Rev. Lett. **109**, 015501 (2012).
[16] M. Gubo, C. Ebensperger, W. Meyer, L. Hammer, K. Heinz, F. Mittendorfer, and J. Redinger, Phys. Rev. Lett. **108**, 066101 (2012).
[17] J. Schoiswohl, S. Agnoli, B. Xu, S. Surnev, M. Sambi, M. Ramsey, G. Granozzi, and F. Netzer, Surf. Sci. **599**, 1 (2005).
[18] F. Allegretti, G. Parteder, L. Gragnaniello, S. Surnev, F. Netzer, A. Barolo, S. Agnoli, G. Granozzi, C. Franchini, and R. Podloucky, Surf. Sci. **604**, 529 (2010).
[19] L. Gragnaniello, G. Barcaro, L. Sementa, F. Allegretti, G. Parteder, S. Surnev, W. Steurer, A. Fortunelli, and F. P. Netzer, J. Chem. Phys. **134**, 184706 (2011).
[20] A. Rota, S. Altieri, and S. Valeri, Phys. Rev. B **79**, 161401 (2009).
[21] C. Hagendorf, R. Shantyr, K. Meinel, K.-M. Schindler, and H. Neddermeyer, Surf. Sci. **532–535**, 346 (2003).
[22] S. Shaikhutdinov, M. Ritter, and W. Weiss, Phys. Rev. B **62**, 7535 (2000).
[23] M. De Santis, A. Buchsbaum, P. Varga, and M. Schmid, Phys. Rev. B **84**, 125430 (2011).
[24] C. Wu, M. S. J. Marshall, and M. R. Castell, J. Phys. Chem. C **115**, 8643 (2011).
[25] M. Gubo, C. Ebensperger, W. Meyer, L. Hammer, and K. Heinz, Phys. Rev. B **83**, 075435 (2011).
[26] M. Finazzi, A. Brambilla, L. Duò, G. Ghiringhelli, M. Portalupi, F. Ciccacci, M. Zacchigna, and M. Zangrando, Phys. Rev. B **70**, 235420 (2004).
[27] A. Brambilla, A. Picone, M. Finazzi, L. Duò, and F. Ciccacci, Surf. Sci. **605**, 95 (2011).
[28] J. Middeke, R.-P. Blum, M. Hafemeister, and H. Niehus, Surf. Sci. **587**, 219 (2005).
[29] K. Amemiya and M. Sakamaki, Appl. Phys. Lett. **98**, 012501 (2011).
[30] S. S. Parihar, H. L. Meyerheim, K. Mohseni, S. Ostanin, A. Ernst, N. Jedrecy, R. Felici, and J. Kirschner, Phys. Rev. B **81**, 075428 (2010).
[31] A. Picone, A. Brambilla, A. Calloni, L. Duò, M. Finazzi, and F. Ciccacci, Phys. Rev. B **83**, 235402 (2011).
[32] A. Tange, C. Gao, W. Wulfhekel, and J. Kirschner, Phys. Rev. B **81**, 220404 (2010).
[33] F. Donati, P. Sessi, S. Achilli, A. Li Bassi, M. Passoni, C. S. Casari, C. E. Bottani, A. Brambilla, A. Picone, M. Finazzi, L. Duò, M. I. Trioni, and F. Ciccacci, Phys. Rev. B **79**, 195430 (2009).
[34] A. Picone, G. Fratesi, A. Brambilla, P. Sessi, F. Donati, S. Achilli, L. Maini, M. I. Trioni, C. S. Casari, M. Passoni, A. Li Bassi, M. Finazzi, L. Duò, and F. Ciccacci, Phys. Rev. B **81**, 115450 (2010).
[35] A. Picone, G. Bussetti, M. Riva, A. Calloni, A. Brambilla, L. Duò, F. Ciccacci, and M. Finazzi, Phys. Rev. B **86**, 075465 (2012).

[36]A. Brambilla, A. Calloni, A. Picone, M. Finazzi, L. Duò, and F. Ciccacci, Appl. Surf. Sci. (2012), doi: 10.1016/j.apsusc.2012.08.067.
[37]P. Blonski, A. Kiejna, and J. Hafner, Surf. Sci. **590**, 88 (2005).
[38]W. A. A. Priyantha and G. D. Waddill, Surf. Sci. **578**, 149 (2005).
[39]A. Pancotti, A. Siervo, M. Carazzolle, R. Landers, and G. Kleiman, Top. Catal. **54**, 90 (2011).
[40]L. Zhang, M. Kuhn, and U. Diebold, Surf. Sci. **375**, 1 (1997).
[41]K. B. Chetry, M. Pathak, P. LeClair, and A. Gupta, J. Appl. Phys. **105**, 083925 (2009).
[42]D. Guo, Q. Guo, M. S. Altman, and E. G. Wang, J. Phys. Chem. B **109**, 20968 (2005).
[43]A. Maetaki and K. Kishi, Surf. Sci. **411**, 35 (1998).
[44]J. Pantförder, R. Domnick, C. Ammon, G. Held, and H.-P. Steinrück, Surf. Sci. **480**, 73 (2001).
[45]S. R. Chubb and W. E. Pickett, Phys. Rev. Lett. **58**, 1248 (1987).
[46]One equivalent monolayer (1 ML) equals the amount of Cr atoms required to completely saturate the adsorption sites on the Fe substrate, i.e., about 12.2×10^{14} atoms/cm^2.
[47]A. Calloni, A. Picone, A. Brambilla, M. Finazzi, L. Duò, and F. Ciccacci, Surf. Sci. **605**, 2092 (2011).
[48]J. P. Perdew, K. Burke, and M. Ernzerhof, Phys. Rev. Lett. **77**, 3865 (1996).
[49]D. Vanderbilt, Phys. Rev. B **41**, 7892 (1990).
[50]P. Giannozzi, S. Baroni, N. Bonini, M. Calandra, R. Car, C. Cavazzoni, D. Ceresoli, G. L. Chiarotti, M. Cococcioni, I. Dabo, A. D. Corso, S. de Gironcoli, S. Fabris, G. Fratesi, R. Gebauer, U. Gerstmann, C. Gougoussis, A. Kokalj, M. Lazzeri, L. Martin-Samos, N. Marzari, F. Mauri, R. Mazzarello, S. Paolini, A. Pasquarello, L. Paulatto, C. Sbraccia, S. Scandolo, G. Sclauzero, A. P. Seitsonen, A. Smogunov, P. Umari, and R. M. Wentzcovitch, J. Phys.: Condens. Matter **21**, 395502 (2009).
[51]H. J. Monkhorst and J. D. Pack, Phys. Rev. B **13**, 5188 (1976).
[52]J. Tersoff and D. R. Hamann, Phys. Rev. B **31**, 805 (1985).
[53]A. Davies, J. A. Stroscio, D. T. Pierce, and R. J. Celotta, Phys. Rev. Lett. **76**, 4175 (1996).
[54]Z. Novotný, G. Argentero, Z. Wang, M. Schmid, U. Diebold, and G. S. Parkinson, Phys. Rev. Lett. **108**, 216103 (2012).
[55]M. Schmid, G. Leonardelli, M. Sporn, E. Platzgummer, W. Hebenstreit, M. Pinczolits, and P. Varga, Phys. Rev. Lett. **82**, 355 (1999).
[56]A. G. Sault, Appl. Surf. Sci. **74**, 249 (1994).
[57]P.-O. Löwdin, J. Chem. Phys. **18**, 365 (1950).
[58]J. Goniakowski and C. Noguera, Phys. Rev. B **79**, 155433 (2009).
[59]A. Eichler and J. Hafner, Phys. Rev. B **62**, 5163 (2000).
[60]W. H. Cloud, D. S. Schreiber, and K. R. Babcock, J. Appl. Phys. **33**, 1193 (1962).
[61]C. Franchini, R. Podloucky, F. Allegretti, F. Li, G. Parteder, S. Surnev, and F. P. Netzer, Phys. Rev. B **79**, 035420 (2009).
[62]S. Agnoli, M. Sambi, G. Granozzi, A. Atrei, M. Caffio, and G. Rovida, Surf. Sci. **576**, 1 (2005).
[63]L. Gavioli, E. Cavaliere, S. Agnoli, G. Barcaro, A. Fortunelli, and G. Granozzi, Prog. Surf. Sci. **86**, 59 (2011).